Modelling the electrochemical transients during repassivation under open-circuit conditions in a neutral solution

Bojan Zajec*, Tadeja Kosec, Andraž Legat

Slovenian National Building and Civil Engineering Institute, Dimičeva 12, Ljubljana SI-1000, Slovenia

A B S T R A C T

The responses of the current and the coupled potential to rapid depassivation have been studied on a three-electrode system under open-circuit conditions. Passivated AISI 304 stainless steel in low- and high-conductivity solutions of Na_2SO_4 has been depassivated with a single, rapid scratch over the small fraction of surface of the working electrode (WE). Single- and dual-WE configurations have been implemented. Once the surface is scratched, the current and potential transients exhibit a delayed maximum and minimum, respectively, in contrast to the outcome of more common potentiostatic scratching experiments. A simple model based on the equivalent circuit has been developed to predict the observed transients and provides clear relations between the features of the transient and the parameters of the electrolyte and the electrodes. The interfacial capacitance of the electrodes' passive surfaces proves crucial for the shapes of the observed potential and current transients. It is shown that this capacitance temporarily provides the majority of the charge for repassivation under open-circuit conditions. Possible sources of specific discrepancies between the model and the measured transients are indicated.

1. Introduction

The ability of certain metals to form a passive layer has been identified as one of the fundamentals of our metal-based civilization [1]. The kinetics of repassivation plays an important role, when the passive film is mechanically disrupted, for example in corrosion fatigue and stress-corrosion cracking (SCC) [2–4]. After the mechanical breakdown of the passive layer, the electrode potential of the metal changes with time according to the electrochemical processes on its surface [5]. The amplitude of the potential fluctuation is related to the ratio between the depassivated area and the entire surface area, and is negligible when a large object suffers a small scratch [5,6].

In contrast to open-circuit conditions, the majority of publications report on investigations of the repassivation kinetics made under potentiostatic control [7–16] where the main observable is the current transient supplied by the potentiostat to keep the scratched electrode at the preselected fixed potential. The potentiostat therefore acts as an external source of the charge needed for the passivation. Such a potentiostatic approach is also found in tribocorrosion and wear-related studies [17], where the scratch is usually made continuously with a pin-on-disk configuration [18].

Since the formation of an oxide layer is normally a very rapid reaction, the mechanical removal of the existing passive layer with a single scratch should occur in the shortest possible time: the bare surface should be created very quickly to avoid simultaneous activation and repassivation [7,19]. In addition to scratching, several other methods have been employed to create a bare surface, such as breaking the electrode in the form of a thin film [7], a guillotined electrode [16,20], laser ablation [14,21] and the potential-step method [15,22].

From experiments conducted under potentiostatic control, various quantities, such as the peak current density and the charge density supplied by the potentiostat versus the applied potential, are the most easily determined. Assuming a certain model for the current-decay curve, the characteristic time of the repassivation, which is closely related to the oxide-growth kinetics, can be obtained as well [8,9,12]. However, in investigations of repassivation under potentiostatic control, specific concerns have to be taken into account [12]: the IR-drop due to large initial currents creates a short-term deviation from the fixed potential [11,15], unless the potentiostat is capable of very rapid IR drop compensation [23]. Irrespective of the IR compensation, the potentiostat's rapid response time also plays a crucial role in ensuring a stable potential. A slow rate of depassivation also impacts on the magnitude of the measured current peak [7,12]. In a few studies the open-circuit

* Corresponding author.
  E-mail address: bojan.zajec@zag.si (B. Zajec).

potential of the depassivated electrode was monitored under galvanostatic conditions [20,22,24] to obtain additional information.

There are very few publications where a constant potential or current was not imposed during the repassivation experiment. Among these, most often the potential of the electrode having its entire surface depassivated was monitored versus time [20,25–28]. In all these studies special attention was paid so that only the newly formed surface was exposed to the solution. Such an arrangement simplifies the interpretation of the potential's evolution as the entire electrode surface is identical. Burstein and Cinderey [20,25,26] guillotined a wire electrode enclosed in a PTFE sleeve, which resulted in the instant formation of a bare surface with a known area. Stoudt et al. [28] applied a single scratch to a flat electrode coated with a thin layer of lacquer. A unique approach was adopted by Chen [27], where an entire rotating-disk electrode was pressed towards a polishing pad and then suddenly moved away from it while remaining in the electrolyte. A more general case was investigated by Oltra et al. [14,21] who investigated the transient of the coupling current between a laser-depassivated and an adjacent electrode, and the transient of their potential.

In contrast to the common potentiostatic scratching experiment we conducted a scratching experiment under open-circuit conditions to simulate field conditions where the object is normally not polarized. For this purpose a measurement technique with three macrosopic electrodes that is commonly used for electrochemical noise measurements [29–33] was employed. The current transient between two electrodes, when one of them suffers a single rapid scratch on a small area, was measured along with the resulting potential transient. The focus of the study was on the time evolution of the single transient rather than on the random high-frequency fluctuations. Several studies [34–37] using an identical experimental arrangement investigated metastable pitting and the transition to stable pits under an open-circuit potential. A similar experimental setup was also implemented to study the initiation and evolution of stress-corrosion cracking (SCC) [38–40]. While the initiation and nucleation of pits and cracks are mostly unpredictable processes, the creation of a bare surface with a scratch is a controlled and well-defined event.

The aim of the paper is to measure, describe and explain the observed current and potential transients that occur due to a single scratch under open-circuit conditions and the origin of the delayed response of the observed signals. In contrast to the studies where the entire surface was depassivated, here the creation of two distinct surfaces (passive and scratched) lead to more complicated behaviour. Our initial observations indicated the crucial role of the passive surface's interfacial capacitance. To verify this, a model based on the equivalent circuit was developed that predicts the observed transients and gives clear relations between the features of the transient and the electrochemical parameters of the electrodes. An attempt to explain the possible sources of specific discrepancies between the model and the measured transients was made.

2. Experimental

The setup consisted of three electrodes: WE1, WE2 and the reference electrode. WE1 is the electrode being scratched. The current between WE1 and WE2 was measured using a zero-resistance ammeter (ZRA), which means they were literally short-circuited, Fig. 1. The potential of these coupled electrodes was measured with respect to the reference electrode at a distant location as recommended for potentiostatically controlled scratching experiments [11]. The sampling frequency of the current and the potential measurement was 50 Hz. No anti-aliasing filter has been applied in order not to alter the shape of fast transients. The ZRA and the high-impedance voltmeter are two modules of a dedicated
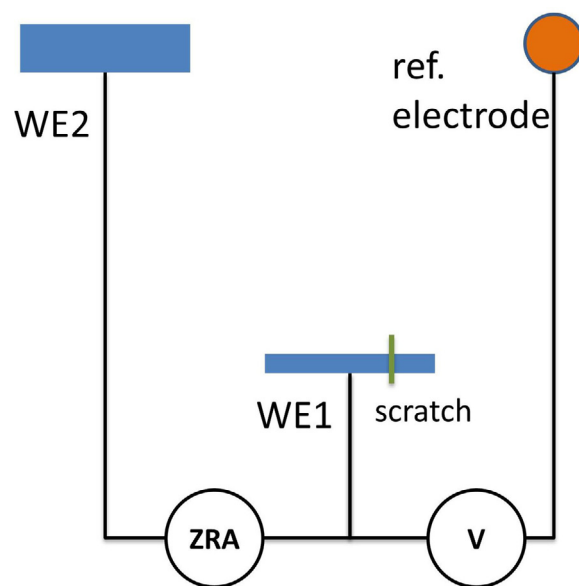

Fig. 1. Scheme of the experimental setup. Distances between electrodes not to scale.

electrochemical-noise-measurement instrument (IPS Elektroniklabor GmbH & Co. KG, Germany).

Electrodes WE1 and WE2 were cut from a 3-mm-thick AISI 304 plate and mounted in epoxy resin. The exposed surfaces were 4 mm × 35 mm ($A_{WE1} = 1.4$ cm^2) and 10 mm × 35 mm ($A_{WE2} = 3.5$ cm^2) for WE1 and WE2, respectively. Each electrode had a cable connection at the backside sealed in epoxy resin. Both working electrodes were abraded with 600-grit SiC paper and rinsed in demineralised water prior to immersion in the electrolyte.

All the experiments were conducted in dilute solutions of Na_2SO_4 at several concentrations, resulting in the electrical conductivity σ ranging from 5.8 up to 1400 μS/cm. Na_2SO_4 was selected as the supporting electrolyte since it does not promote localized corrosion at low concentrations [11] and is free from halide ions that negatively influence the formation of the passive film already at low concentrations. Likewise, the saturated mercury sulphate reference electrode (SMSE) was chosen. All the experiments were performed at room temperature, while the electrolyte (approximately 3 L) was in contact with the ambient air. All three electrodes were positioned at the corners of an equilateral triangle with a side of approximately 14 cm, ensuring mutual distances much larger than the dimensions of the scratch. Each scratching experiment was conducted after at least overnight exposure of freshly ground electrodes in the electrolyte of interest, thus forming a native passive film and a stable electrode potential.

The scribe used was a thin sharp blade made of non-conductive ceramic. A single rapid scratch was made with an electromagnet-based mechanism. The blade's movement time was 6 ms. The blade transversed the 4-mm-wide WE1 electrode by starting and finishing its movement in the surrounding resin. The scratch was approximately 40 μm wide, hence the scratched area $A_{scratch} = 0.0016$ cm^2 represents around 0.11% of the surface of WE1. The experimental setup consisted of a fully plastic (ABS) holder for all three electrodes. Triggering the scribe movement slightly above the electrode surface did not cause any hydrodynamic noise in the current or potential signal.

Measurements for the following two electrode configurations are investigated in the paper:

- single-WE configuration, where WE2 was disconnected, only the potential signal of WE1 was recorded.
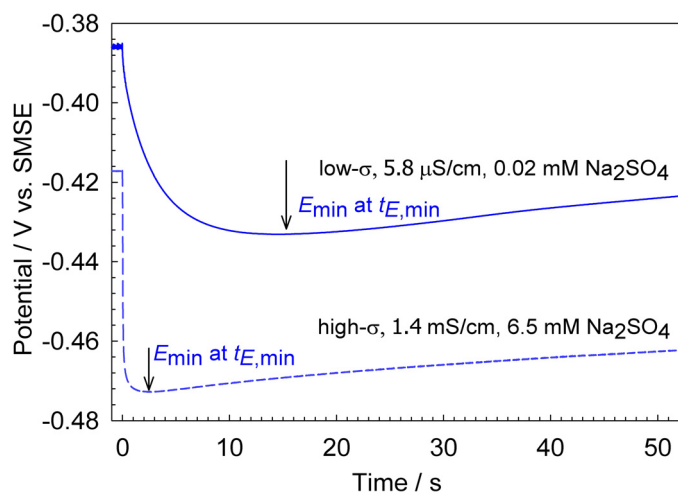
Fig. 2. Potential transients of single-WE configuration for electrolyte with 5.8 µS/cm (low-σ) and for 1.4 mS/cm (high-σ) conductivity.

- dual-WE configuration, consisting of WE1, WE2 and a reference electrode as depicted in Fig. 1. Current and potential signals were recorded.

Besides scratching experiments, a dedicated set of measurements was carried out to determine the interfacial capacitance of the electrodes' passive surfaces since this quantity is needed in the forthcoming model. This was done for electrodes WE2 and WE1, prepared in the same way as described before. Two different techniques were applied: electrochemical impedance spectroscopy (EIS) and galvanostatic charge/discharge (GCD) techniques [41,42]. For EIS a classic three-electrode system with a Pt-foil as the counter electrode and an Ag/AgCl reference electrode inserted in a Luggin capillary were applied. A Gamry 600 potentiostat, expanded with a Gamry Instruments framework module for the EIS measurements, was used. The measurements were conducted at the open circuit potential (OCP) in the frequency range 10 kHz to 1 mHz with five points per decade. The amplitude of the voltage perturbation was 7 mVrms ($\approx$ 10 mV peak amplitude). GCD (also known as chronopotentiometry) was performed using the same experimental setup but just for the WE2 electrode. Eight cycles of positive / negative DC current with identical magnitudes were applied while the WE potential was monitored. Several measurements were carried out with the current magnitude in the range from 50 nA to 1 µA while the cycle period was adjusted so that 2 µAs of charge was charged / discharged per half-cycle.

3. Results

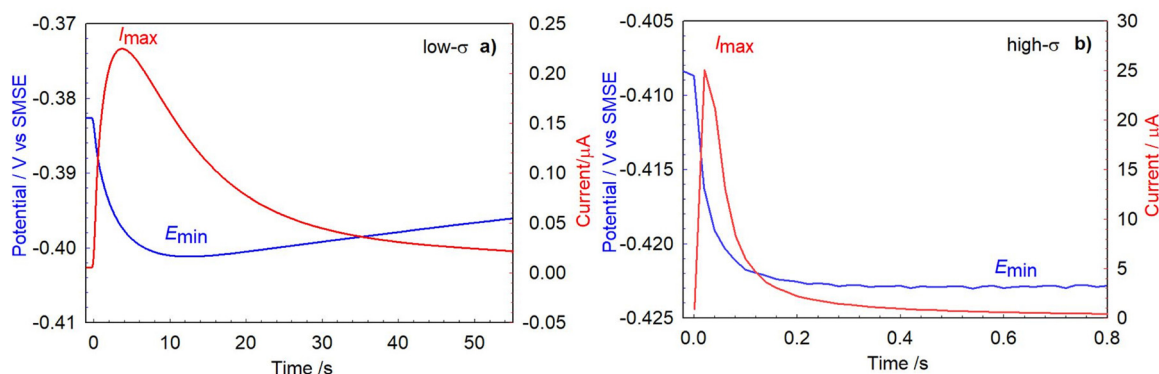In the following, most of the results presented will be limited to the measurements performed in the Na_2SO_4 electrolyte with a conductivity $\sigma = 5.8$ µS/cm (low-σ, conc. 0.02 mM) and $\sigma = 1.4$ mS/cm (high-σ, conc. 6.5 mM).

In Fig. 2 typical potential transients are presented for the single-WE configuration in a low- and a high-σ electrolyte. The rapid scratch is created at $t = 0$ and immediately after that the potential starts to decrease. In the low-σ electrolyte this decrease is slow and the minimum potential value E_{min} is achieved only after $t_{E,min} = 14.5$ s. Afterwards, the potential increases slowly and approaches the initial potential (not show in Fig. 2). In the high-σ case, the potential decrease is initially very rapid and reaches the minimum much earlier; however, the potential recovery follows the same slow increase as in the low-σ electrolyte. The amplitude of the negative peak $\Delta E = E(t < 0) - E_{min}$ was not found to be dependent on σ and was always around 50 mV for the single-WE configuration.

In Fig. 3 typical current and potential transients are presented for the dual-WE configuration in a low- and a high-σ electrolyte. Once the surface is scratched, the current signal $I(t)$ is not at its maximum but only starts to increase and achieves the peak value I_{max} at time $t_{I,max}$, and then decreases at a slower rate. The time of the current peak $t_{I,max}$ is of the order of seconds for low-σ, while it reduces to a few 10s of ms for the high-σ electrolyte. The sign of the current indicates that WE1 behaves as the anode for the whole duration. This is also reflected in the potential that rapidly decreases after the scratch and achieves a minimum value before it begins to rise very slowly, similar to the behaviour in the single-WE configuration. This recovery to the initial potential value is significantly slower than the $I(t)$ signal recovery. It should be noted that in the dual-WE configuration the amplitude of the negative peak ΔE is considerably smaller, only around 15 mV and the potential minimum is achieved earlier in comparison to the dual-WE configuration. The current peak was always observed to precede the potential minimum ($t_{I,max} < t_{E,min}$), irrespective of the conductivity. On the other hand, the increased conductivity clearly results in shorter rise and fall times for the current transient and the fall time of the potential, Fig. 3b. It also significantly increases the magnitude of the current peak from 0.23 µA to 25 µA, but was not observed to impact on the amplitude of the negative peak ΔE.

Despite our best efforts to perform the scratching experiment under identical conditions, the results show a relatively large scatter, which was observed during repetitions of the experiments. For this reason, only large differences in the results obtained from varying the configuration or conductivity could be indisputably linked to a modification of the experimental parameters. One possible source of the observed scatter is the scratching mech-

Fig. 3. Potential and current transients for dual-WE configuration for electrolyte with a) 5.8 µS/cm and b) for 1.4 mS/cm conductivity.

anism that involves the blade which might not provide identical scratches. Moreover, the relatively poor reproducibility of such scratching measurements seems to be inherent of this kind of depassivation as reported in other studies [8,11], though the scatter itself was rarely quantified.

In order to determine the interfacial capacitance, besides the scratching experiments also EIS and GCD measurements under the stationary conditions were performed. Obtained EIS data were fitted with a simple equivalent circuit where the charge-transfer resistance is in parallel with the constant-phase element (CPE), with both of them being in series with the electrolyte resistance. The impedance of the CPE is $Z(CPE) = 1/[Y_0(i\omega)^n]$, which represents the behaviour of the passive surface's interfacial capacitance. If $n = 1$ the CPE becomes an ideal capacitor with the capacitance Y_0. For low-σ the fit is very good and the interfacial capacitance per unit area c is around 25 µF/cm^2, with $n \approx 0.9$, i. e. close to unity. For high-σ the fit is poorer and $c \approx 45$ µF/cm^2. From GCD data the integral form of the capacitance [41] was determined from the quotient of the charge and the change of the electrode potential in the last charging / discharging cycle. For low-σ the average is $c \approx 30$ µF/cm^2, while for high-σ it is $c \approx 39$ µF/cm^2.

4. Modelling

4.1. Impact of the capacitance

To establish the model it is first necessary to identify the relevant processes and factors as well as the underlying physical relations. In the potentiostatic scratching experiment the current supplied by the potentiostat is directly related to the current needed for the dissolution of the metal and subsequent repassivation of the scratch. In our case, where the scratch is made under open-circuit conditions, the measured $E(t)$ and $I(t)$ transients apparently do not offer such a simple interpretation as in the potentiostatic case. In particular, the obvious delay of the potential minimum and the current peak after the scratch (in the dual-WE configuration) contrasts with the current transient observed under potentiostatic conditions where the transient achieves its maximum immediately after the scratch is formed.

The observed delay was assumed to be related to the capacitance of the electrochemical interface separating the passive surface and the electrolyte, as proposed by Isaacs and Cho [43,44]. The cathodic reactions, such as oxygen reduction in a neutral electrolyte, are, however, too slow to provide enough current and the majority of the charge required for the repassivation is temporarily obtained from the passive surface's interfacial capacitance. Due to this non-faradaic process, the mixed-potential theory is strictly only valid as an average over time and not at any instant. It is the discharge of this capacitance that leads to a decrease of the potential [43,44]. The amplitude of the negative peak ΔE in our measurements was observed to depend heavily on the available passive area of the electrode(s), which is further dependent on the configuration. Besides the single-WE and dual-WE configurations, a reduced dual-WE configuration was also partially examined, where the area of WE2 was reduced to 0.4 cm^2. Our measurements indicated that the product of the amplitude of the negative peak ΔE and the area of the electrode(s) is roughly constant. For nominally identical scratches that consume the same amount of charge for repassivation, the charge $c(A_1 + A_2)\Delta E$ being taken from the electrodes' capacitance, should also be constant. Here, the symbol c denotes the interfacial capacitance per unit area. Therefore, ΔE should be proportional to $(A_1 + A_2)^{-1}$, irrespective of the configuration. This relation was indeed confirmed by our measurements. Moreover, the electrolyte's conductivity σ was observed to have no apparent influence on ΔE.
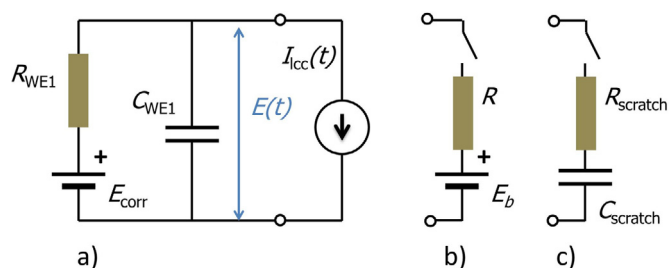
Fig. 4. Equivalent electrical circuit for the single-WE configuration with (a) general current sink electrical analogue of the scratch, (b) electrical analogue of the scratch introduced by Isaacs et al. for metastable pitting [34], and (c) electrical analogue of the scratch with initially charged capacitor used in our model.

4.2. Model for single-WE configuration

The modelling of electrochemical transients was usually approached by considering the electrical circuit analogue of the metal-electrolyte interface. In such a manner Isaacs et al. [34] investigated the evolution of the potential transient during the pitting of stainless steel under the open-circuit conditions. The authors presented a simple equivalent electrical circuit, representing the relevant electrochemical process on the electrode, and related the circuit elements with certain electrode parameters. However, their model does not predict the duration of metastable pit growth. Oltra et al. investigated [14,21,45] a setup with two electrodes arranged as a disc and a ring with the former fully depassivated by a laser pulse. The potentiostatically controlled and open-circuit cases were examined. For the latter, the current between the two electrodes and their coupled potential were measured. In all three papers the authors used identical equivalent circuit for the passive surface as was used by Isaacs et al. The same circuit is used in our model where the electrochemical properties of the passive surface of the electrode WE1 are represented by the capacitor C_{WE1} being in parallel with the DC voltage source and the resistor, Fig. 4a. The capacitor represents the electrode's interfacial capacitance. The DC source voltage is equal to the corrosion potential E_{corr} of the unscratched passive surface [34,35]. The resistor R_{WE1} represents the impedance of the cathodic (oxygen reduction) and the anodic (passive film growth) reactions at the low-frequency limit, i.e., the charge-transfer resistance on the WE1's passive surface. In this way the electrochemical polarization is represented linearly, and therefore the model is only valid for small deviations from E_{corr}.

The rightmost branch in Fig. 4a represents the influence of the scratch, which is a small, bared surface behaving as a localized anode. In general, it can be represented as a current sink that is consuming the localized corrosion current $I_{lcc}(t)$, which is time dependent in the case of the scratch that repassivates (current is zero before scratching and after the scratch repassivation). However, $I_{lcc}(t)$ is not known per se and as such does not allow for a simple mathematical treatment of the circuit.

Isaacs at al., who studied metastable pitting [34] simply used a resistor in series with an additional DC voltage source, having the potential of the bare surface E_b, (which is lower than the OCP of the passive surface E_{corr}), since the area inside the pit remains active during the pit growth, Fig. 4b. The pit initiation and repassivation were modelled in a very simplified manner, by closing and opening a manual switch in that branch. This requires a knowledge of the pit growth duration, making it unacceptable for our case. The resistor represents the solution's electrical resistance to the growing pit.

In our case, where the scratch repassivates, an electrical analogue that consumes a finite amount of charge is needed. The bared surface should thus be represented as a current sink with

a finite charge capacity that is initially at E_b; however, its potential increases [20,25] during the repassivation towards E_{corr} of the passive surface. During this process increasingly less current is being consumed. To satisfy these requirements and to keep the circuit simple, we decided to investigate whether the behaviour of the bare surface could be represented by an ideal capacitor $C_{scratch}$, having an initial voltage at E_b, Fig. 4c. The voltage on the capacitor $C_{scratch}$ therefore represents the time-dependent potential in the scratched area and the current passing through $R_{scratch}$ represents the localized corrosion current consumed by the oxide growth in the scratch. A similar idea was suggested by Oltra et al. [21] where the bared area was represented by a DC voltage source and an uncharged capacitor in series, but no detailed description of these elements was given. Their representation is identical to our charged capacitor with its initial voltage equal to that of their DC voltage source. It needs to be stressed here that the value of $C_{scratch}$ is not related to the interfacial capacitance of the scratched area, but to the required repassivation charge that is of the order of mAs/cm^2 [8,9,22,46,47] for stainless steel. The charge $C_{scratch}(E_{corr} - E_b)$ is the charge required for repassivation. The flow of the charge between the passive surface of WE1 and the bare surface is obstructed by the electrolyte's electrical resistance, represented by the resistor $R_{scratch}$. Its actual value depends on the scratch's shape and dimensions, and the electrolyte's conductivity σ. The solution's resistance to the long rectangular scratch of negligible depth is [48]

$$R_{scratch} = \frac{\ln(4b/a)}{2\pi\sigma b}, \tag{1}$$

where the scratch width is $2a$, the length is $2b$ and $b \gg a$.

Prior to the scratch the switch in Fig. 4c is open and the rightmost branch is absent from the equivalent circuit while C_{WE1} is charged to E_{corr}. Immediately after the instant scratch (at $t = 0$) the switch is closed and this branch appears with $C_{scratch}$ initially charged to $E_b = E_{corr} - U_0$ (where $U_0 > 0$). The passive surface starts providing the current through $R_{scratch}$ and its potential $E(t)$ decreases [34] until $t_{E,min}$, when the voltages of both capacitors are almost equal. By this time the scratch can be deemed as repassivated [43,44]. The resistance of R_{WE1} needs to be high compared to $R_{scratch}$ so that the DC voltage source (cathodic processes) has little influence during the initial potential decrease and starts playing an important role only near $t_{E,min}$ and particularly afterwards, as it slowly recharges both capacitors back to the E_{corr} potential.

For the proposed equivalent circuit, Fig. 4a and 4c, the actual value of E_{corr} is irrelevant for the mathematical modelling of the circuit's behaviour. It only defines the additive constant of the potential $E(t)$, so we can set $E_{corr} = 0$ V and therefore omit the DC voltage source from the circuit. The initial voltage across $C_{scratch}$ is then $-U_0$.

From the principal equations for current and voltage a set of two differential equations is obtained and the solution for $E(t)$ is:

$$E(t) = -\frac{U_0 C_{scratch} R_{WE1}}{\sqrt{\alpha^2 - 4\beta}} \left(\exp\left(-\frac{\alpha - \sqrt{\alpha^2 - 4\beta}}{2\beta} t \right) \right.$$
$$\left. - \exp\left(-\frac{\alpha + \sqrt{\alpha^2 - 4\beta}}{2\beta} t \right) \right) \tag{2}$$

where $\alpha = C_{WE1}R_{WE1} + C_{scratch}R_{WE1} + C_{scratch}R_{scratch}$ and $\beta = C_{WE1}C_{scratch}R_{WE1}R_{scratch}$ The signal $E(t)$ has two time constants that are complicated functions of the circuit elements' properties. It will be revealed later that for our case of a small scratch and a large passive area $C_{WE1} \gg C_{scratch}$ and that $R_{WE1}C_{WE1} \gg R_{scratch}C_{scratch}$ so $\alpha^2 \gg 4\beta$. Using these relations certain approximations and simplifications can be made that lead to the following characteristic

times:

$$\frac{\alpha - \sqrt{\alpha^2 - 4\beta}}{2\beta} \approx \frac{1}{\alpha} \approx \frac{1}{(C_{WE1} + C_{scratch})R_{WE1}} = \frac{1}{\tau_r} \tag{3}$$

and

$$\frac{\alpha + \sqrt{\alpha^2 - 4\beta}}{2\beta} \approx \frac{\alpha}{\beta} \approx \frac{1}{R_{scratch}C_{scratch}} + \frac{1}{R_{scratch}C_{WE1}} = \frac{1}{\tau} \tag{4}$$

Thus, the time evolution of the potential $E(t)$ given in Eq. (2) can then be then rewritten as

$$E(t) = E_0(\exp(-t/\tau_r) - \exp(-t/\tau)) \tag{5}$$

where

$$E_0 = -\frac{U_0 C_{scratch} R_{WE1}}{\sqrt{\alpha^2 - 4\beta}} \tag{6}$$

and the characteristic times of the potential decrease τ and its recovery τ_r were defined by Eqs. (4) and (3), respectively. The approximations derived in these equations differ by less than one percent from the exact values. Moreover, they bear a physical meaning for both characteristic times; τ can be rewritten as $R_{scratch}C'$ where C' is the equivalent capacitance of C_{WE1} and $C_{scratch}$ wired in series. Time τ is the characteristic time of the circuit without R_{WE1} (in the $R_{WE1} \to \infty$ limit). Similarly, τ_r reflects the recharging of both capacitors ($C_{WE1} + C_{scratch}$) through the R_{WE1} resistor, while neglecting $R_{scratch}$.

In Fig. 5a the fit of expression (5) to the measured $E(t)$ signal for the single-WE, low-σ case is presented. The agreement is very good, and the best-fit parameters are $\tau = 3.7$ s, $\tau_r = 150$ s and $E_0 = -53$ mV. But from these data it is unfortunately not possible to obtain the four unknown values of the circuit elements, which are C_{WE1}, R_{WE1}, $C_{scratch}$ and its initial voltage U_0. Only $R_{scratch} = 822$ kΩ is known from Eq. (1). Additional piece of information is obtained from our interfacial capacitance measurements. These measurements indicated a certain degree of dependence on the electrolyte concentration. For the present purpose an average value of $30\,\mu F/cm^2$ was selected as a compromise to represent the capacitance in the high- and low-σ electrolytes. This results in $C_{WE1} = 42\,\mu F$. Now, the Eqs. (3), (4) and (6) can be solved and yield: $C_{scratch} = 5.04\,\mu F$, $R_{WE1} = 3.19$ MΩ and $U_0 = 484$ mV. These results

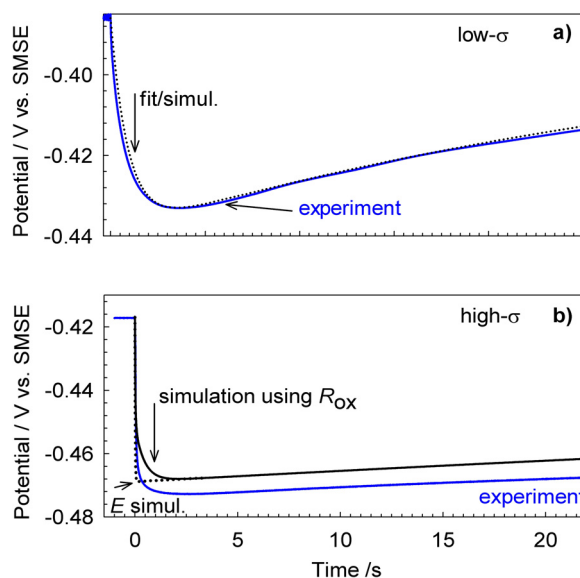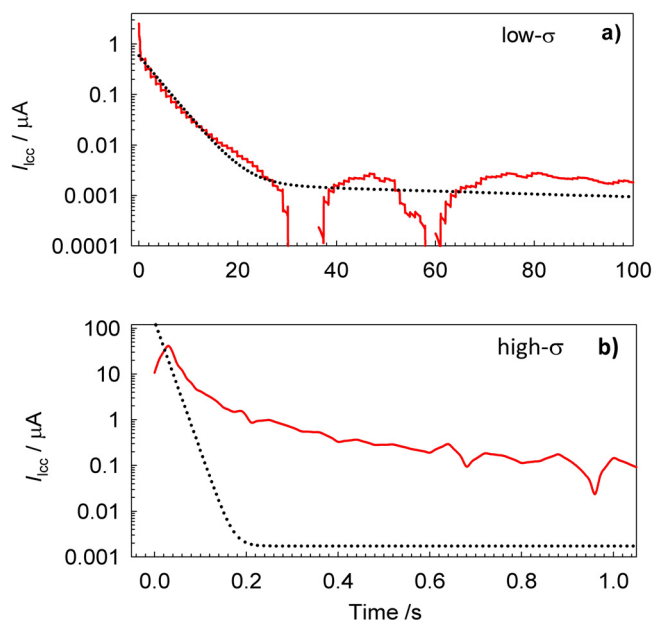**Fig. 5.** Comparison of the simulated and measured $E(t)$ curves a) for the low-σ ($\sigma = 5.8\,\mu S/cm$, $R_{scratch} = 822$ kΩ) and b) high-σ ($\sigma = 1.4$ mS/cm, $R_{scratch} = 3410\,\Omega$) electrolytes in single-WE configuration. Simulation using R_{ox} is explained in the discussion..

Fig. 6. Comparison of the localized corrosion current $I_{lcc}(t)$ derived (Eq. (7)) from the measured $E(t)$ (solid curve) and a modelled one (dotted curve), for a) low-σ electrolyte, single-WE configuration and b) high-σ electrolyte, single-WE configuration.

fall within a sensible range and support the assumptions made during model derivation. The polarization resistance of stainless steel's passive surface follows to be 4.5 MΩ cm^2, and $C' = 4.5\,\mu$F.

The modelled $E(t)$ curves in Fig. 5 and the subsequent diagrams are shifted from the assumed E_{corr} of 0 V to the experimental E_{corr} measured just before the scratch, in order to enable a comparison with the experimental $E(t)$ curves. NGSpice open-source circuit-simulation software [49] was used for the numerical simulation of all the voltage and current transients in this circuit. The analytical approximation given by Eq. (5) differs by less than a linewidth from the numerically simulated $E(t)$.

The simulation for the single-WE, high-σ case was made using the same values of the parameters (obtained in fit in Fig. 5a), except that $R_{scratch}$ was modified to the high-σ electrolyte's conductivity. In Fig. 5b the simulated $E(t)$ for the high-σ ($\sigma = 1.4$ mS/cm, $R_{scratch} = 3410\,\Omega$) electrolyte is presented. The simulated $E(t)$ correctly describes the initially very rapid drop of the potential, but it fails to exhibit the delayed and the broad minimum seen in the experimental curve, so there is only a rough match. Nonetheless, the amplitude of the negative peak ΔE is fairly well predicted and the recovery rate is nearly identical to the measured value.

From the measured potential evolution $E(t)$, the localized corrosion current $I_{lcc}(t)$ can be determined, irrespective of the electrical analogue of the scratch branch. From Kirchhoff's law it follows that [45]

$$I_{lcc}(t) = -C_{WE1}\frac{dE(t)}{dt} - \frac{E(t) - E_{corr}}{R_{WE1}} \tag{7}$$

For the I_{lcc} calculation the parameters C_{WE1} and R_{WE1} of the passive surface need to be known. Using the obtained $C_{WE1} = 42\,\mu$F and $R_{WE1} = 3.19$ MΩ, the localized corrosion current $I_{lcc}(t)$ was calculated from the measured $E(t)$ for the low- and high-σ cases, Fig. 6. For comparison, the $I_{lcc}(t)$ calculated from the corresponding simulated $E(t)$ signal is depicted, too. For the low-σ case, Fig. 6a, both currents are in good agreement despite the scatter in the experimentally obtained curve due to the numerical differentiation. From Eqs. (5) to (7) it follows that I_{lcc} is the sum of two exponential decays. The first one corresponds to the repassivation that ends when the voltages of both capacitors are nearly equal, i.e. around
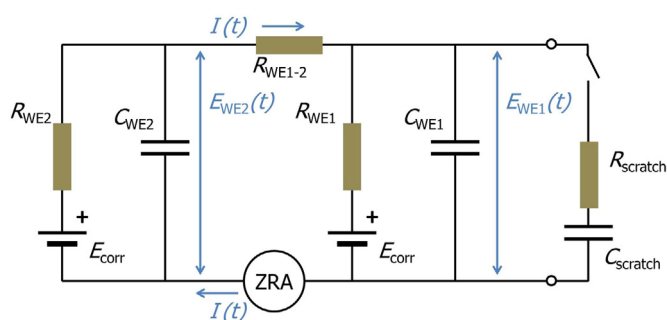
$t_{E,\min}$. Before explaining the second slope, it should be noted that in our model the $C_{scratch}$ remains part of the circuit even after the repassivation, yet the repassivated surface should have a negligible capacitance comparable to the its interfacial capacitance, which is of the order of $cA_{scratch} = 0.05\,\mu$F. After $t_{E,\min}$ the cathodic current passing through R_{WE1} therefore also charges $C_{scratch}$, and not only C_{WE1}. The second slope of I_{lcc} represents this current to $C_{scratch}$. By keeping the scratch branch with $C_{scratch}$ connected even after the repassivation the circuit's behaviour is only slightly altered since $C_{scratch} \ll C_{WE1}$.

For the high-σ case, Fig. 6b, the I_{lcc} from the experimental $E(t)$ exhibits significantly slower and non-exponential decay compared to the modelled one. The agreement can be found only in the first fraction of a second.

4.3. Model for dual-WE configuration

The addition of the electrode WE2 makes it possible to measure the current transient $I(t)$ between WE1 and WE2 after creation of the scratch. This current represents only a part of the current that is flowing to the bared surface [35], since the current contribution from WE1 itself cannot be measured by ZRA.

Only a few publications deal with the modelling of such a dual-electrode system with some kind of localized, time-dependent corrosion on one or both of the electrodes. A model for the system consisting of two identical electrodes with pitting taking place on one of them was proposed by Sasaki and Isaacs [35], where the relationship between the coupling current and the potential was derived. Unfortunately, the authors neglected the effect of the solution's electrical resistance, so the potentials of both electrodes are equal. This simplification is a common one. The ohmic drop in the solution was considered by Danielson [50]. His paper examines the transient response of electrochemical processes simulated by an equivalent circuit to a single noise event. In the following we will follow this model and further adapt it to suit the existing problem.

An equivalent electrical circuit for this configuration is shown in Fig. 7. Due to the complexity of the circuit no analytical solution was sought, and all the modelling results are based on NGSpice numerical solutions [49]. The WE2 electrode is assumed to have identical properties to WE1, adjusted only for the difference in the area. The current I between WE1 and WE2 is obstructed by the solution's resistance which is modelled as a resistor R_{WE1-2}. The true value of the resistance between two electrodes in solution is, in general, a complicated function of geometry. However, for two electrodes in an infinite medium separated by the distance l, which is much larger than their dimensions, the resistance R is given by ref. [51]
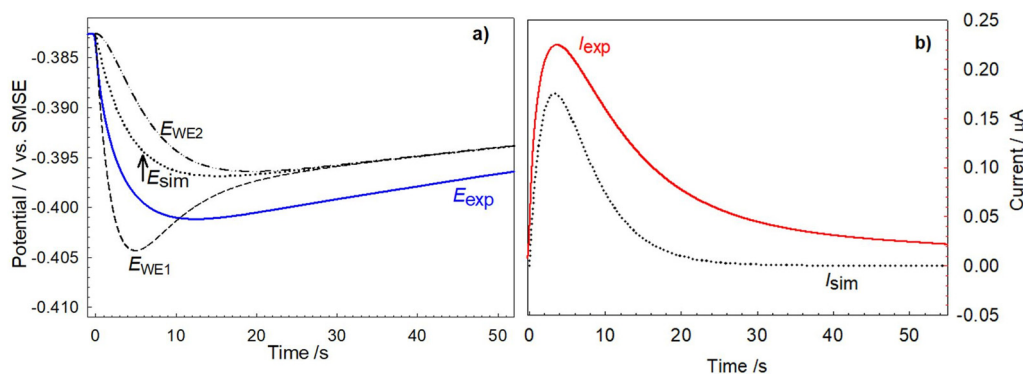
$$R = R_{11} + R_{22} - \frac{1}{2\sigma l}\quad, \tag{8}$$

Fig. 7. Equivalent electrical circuit for the dual-WE configuration.

Fig. 8. Simulated and measured (a) potential transients and (b) current transients for the dual-WE configuration, $\sigma = 5.8\,\mu S/cm$.

where R_{11} denotes the resistance associated with the crossing of the current from the first electrode to the solution and R_{22} the return of the current from the solution to the second electrode. For rectangular electrodes these resistances are given by Eq. (1). From Eqs. (1) and (8) the values of R_{WE1-2} are obtained as $95.2\,k\Omega$ and $394\,\Omega$ for $\sigma = 5.8\,\mu S/cm$ and $1400\,\mu S/cm$, respectively. The R_{WE1-2} is almost nine-times lower than the corresponding $R_{scratch}$, since the areas of both electrodes are large compared to the area of the scratch. It is obvious that the location of the electrodes in the current setup is irrelevant as long the mutual distances are large compared to the dimensions of the scratch and the electrode.

The current I results from the potential difference between the WE2 and WE1 electrodes (more accurately from the difference in the solution potentials at the surfaces of the respective electrodes) hence

$$I = \frac{E_{WE2} - E_{WE1}}{R_{WE1-2}} \tag{9}$$

where E_{WE2} and E_{WE1} are the potentials of the electrodes. While these two potentials can be obtained with a numerical simulation of the circuit, this is not the case in the experiment where only the coupled potential E is measured at the position of the reference electrode. Since the distance to its position is again large compared to the dimensions of the scratch and the electrodes, we attempt to roughly approximate the potential at the reference electrode as an area-weighted average [52,53]

$$E(t) = \frac{1}{A_1 + A_2} \left(A_1 E_{WE2}(t) + A_2 E_{WE1}(t) \right). \tag{10}$$

The comparison of the simulation (using the same model parameters, obtained from the single-WE, low-σ fit, as in the previous section) to the experimental results obtained in the low-σ electrolyte (Fig. 3a) is presented in Fig. 8. The agreement between the measured and simulated curves is quite good, particularly the peak / minimum times $t_{I,max}$ and $t_{E,min}$, which matches well, but the $I(t)$ decays somewhat too rapidly in the simulated case. Also the amplitude of the current and potential peaks in the simulation are somewhat lower compared to the measured ones.

When again applying the same model parameters to simulate signals for high-σ case (with R_{WE1-2} and $R_{scratch}$ adjusted), the agreement is weaker, Fig. 9. The simulated current peak is too high, and the simulated $E(t)$ initially decreases too quickly. On the other hand, the $t_{I,max}$ coincides well and the value of ΔE is reproduced well, too.

A detailed analysis of the simulated voltages and currents in the circuit (Fig. 7, low- and high-σ) reveals that the initial charge for the repassivation comes from the interfacial capacitance of the WE1 electrode, and its potential E_{WE1} rapidly decreases. This leads to a potential difference between both electrodes that gives rise to

the current $I(t)$ that starts discharging the interfacial capacitance of WE2, analogous to the transmission-line effect [54]. Due to this additional source of charge, $E_{WE1}(t)$ reverses earlier and at a less negative potential than the single WE case, Fig. 2. Soon after $t_{I,max}$, WE2 provides a current for the repassivation as well as for the recharging of WE1's interfacial capacitance. Eventually, the potentials of both electrodes are equalized due to the current and they slowly begin to rise due to the cathodic processes enhanced by the decrease of the potential.

Besides the comparison of the $E(t)$ and $I(t)$ temporal evolutions, it is worth comparing the prediction of certain notable quantities such as I_{max}. In Fig. 10 the measured and simulated I_{max} values versus σ are presented for the dual-WE configuration. For the simulated values the relation is $I_{max} \propto \sigma$. This relation should be compared to Eq. (9) where $R_{WE1-2} \propto 1/\sigma$ due to Eqs. (1) and (8). It follows that at the time of the current peak the potential difference in the numerator of Eq. (9) is constant, no matter what the solution conductivity σ. Actually, the experimental datapoints do not deviate much from the predicted linear relationship: the best fit gives $I_{max} \propto \sigma^{0.87}$.

5. Discussion

The aim of the study was to understand the measured current (I) and potential (E) transients under open-circuit condition and the involved electrochemical processes. For this reason, a simple model based on the equivalent circuit was developed and the basic parameters of each element were determined. Such a comprehensive model provided clear relationships between the features of the transients and the parameters of the electrodes and the environment. The model fitted very well to the $E(t)$ transient measured in the single working-electrode (WE) configuration for low-σ (Fig. 5a), whereas the agreement for high-σ was poorer (Fig. 5b) since the shape of the curve is not reproduced.

The main parameters of the elements were assessed, and the obtained values were then implemented in the extended model for the dual-working-electrode configuration. This model was also in good agreement with the measurements, particularly the timing of $t_{I,max}$ and $t_{E,min}$. Larger differences were, however, observed for the transients in the high-σ electrolyte (Fig. 9). Besides the mostly successful prediction of the $E(t)$ and $I(t)$ signal shapes, the model also reproduces the observed independence of the measured ΔE from the electrolyte conductivity. As an illustration, for the single-working-electrode configuration the model-based ΔE is 48.5 mV and 51.8 mV for the low- and high-σ, respectively. For the dual-working-electrode configuration, the corresponding values given the by the model are $\Delta E = 14.0$ mV and 15.4 mV. The variation is undetectable when compared to the experimental scatter: for single-/dual-WE configuration the value of ΔE is 49.4 ± 9.7
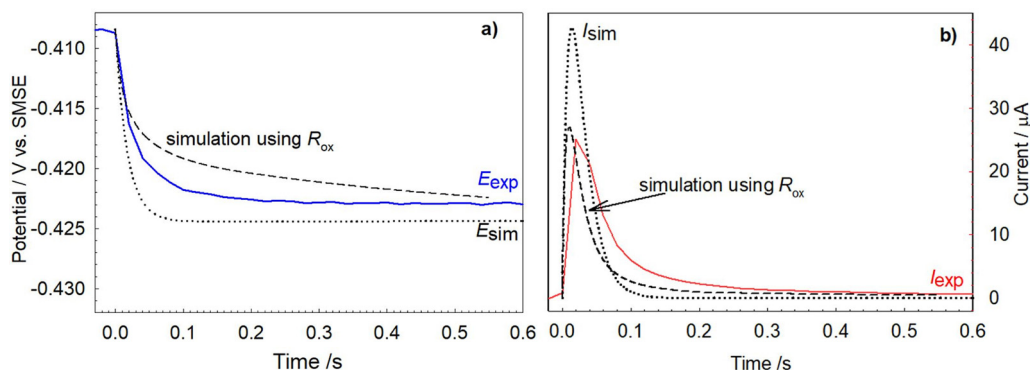
Fig. 9. Simulated and measured a) potential transients and b) current transients for the dual-WE configuration, $\sigma = 1400\,\mu S/cm$. Simulation using R_{ox} is explained in the discussion.
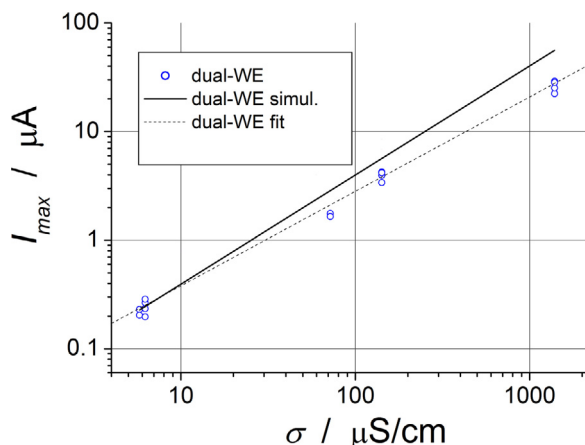
Fig. 10. Comparison of the measured and simulated current peak value I_{max} dependency on the electrolyte conductivity σ.

mV and 15.8 ± 2.8 mV, respectively. These values are the statistics for 6 and 9 measurements performed at four σ values. Similarly, the model prediction of I_{max} for various electrolyte conductivities is also in fairly good agreement with the measurements, as shown in Fig. 10.

Speaking of the comparison between the model and the experimental results it should be noted that the measured $E(t)$ and $I(t)$ curves were not fully reproducible, and therefore some disagreement between the model prediction and the experimental results (particularly in terms of the peak and minimum amplitudes) is to be expected. Yet certain systematic deviations do exist and need to be discussed in more detail. The striking disagreement in $t_{E,min}$ in the single-WE configuration at high-σ, Fig. 5b, clearly cannot be eliminated by applying some better parameters in Eq. (5). The observed mismatch between the curves suggests a stronger impediment of the current to the scratch $I_{lcc}(t)$ once the potential approaches its minimum in order to have it delayed and broadened. This is evidently revealed in Fig. 6b where the measurement-based $I_{lcc}(t)$ decreases significantly more slowly compared to the model and does not even follow the assumed exponential decay, except for the first decade of the current decrease. Despite the significant difference in the $I_{lcc}(t)$ curves, the charge consumed by the scratch up to $t_{E,min}$ matches very well. The time integral of $I_{lcc}(t)$ is 2.2 and 2.3 μAs for the modelled and experimental cases, respectively.

Using an ideal capacitor $C_{scratch}$ to mimic the electrochemical properties at the repassivating surface is an obvious simplification, yet it still reproduces the main features of the observed transients. In addition, it allowed a relatively simple circuit representation, and for the single WE an explicit mathematical expression

could be obtained. According to this simple model the potential at the growing oxide layer initially increases as does the voltage on $C_{scratch}$ for the single- and dual-WE configurations. For the scratch electrical analogue we should, ideally, apply an electrical element for which the voltage and impedance are representative of the growing oxide layer at a particular moment, with most likely each of them being a function of the accumulated charge. Such an attempt, albeit rudimentary, is presented in the next paragraph.

It was hypothesized that the electrical resistance of the growing oxide layer could be responsible for this delayed minimum, Fig. 5b. This assumption was verified with the modified single-WE circuit where an additional, time-dependent, resistor R_{ox} was put in series with the existing $R_{scratch}$, Fig. 4c. Its value represents an additional electrical resistance due to the growing oxide layer. The reasoning for the selection of any of the known growth models is definitely beyond the scope of this paper. Therefore R_{ox} was modelled in the simplest possible way – to increase linearly with time from zero up to a certain ceiling value;

$$R_{ox.} = \min(t \cdot 500\,\text{k}\Omega/\text{s}, 100\,\text{k}\Omega) \tag{11}$$

The application of R_{ox} with the rate of $500\,\text{k}\Omega/\text{s}$ and ceiling value of $100\,\text{k}\Omega$ yields significantly better match of $E(t)$ for the single-WE configuration at high-σ, Fig. 5b. This additional time-dependent resistance reproduced the measured shape of the curve around E_{min} very well. A similar situation could be argued for the dual-WE in high-σ, where the insertion of the same R_{ox} results in a significantly better agreement in terms of I_{max} and the decreasing of the current and potential, Fig. 9. For low-σ configurations the addition of such R_{ox} is negligible since $R_{scratch} = 822$ kΩ is substantially higher than the maximum R_{ox} of 100 k Ω. It appears that the model without R_{ox} is acceptable as long as the electrolyte's resistance is the main bottleneck for the current transfer to the scratch.

An additional reason for the weaker agreement between the simulation and the high-σ measurements is likely the adoption of the identical passive surface properties C_{WE} and R_{WE} for all the electrolyte concentrations. Furthermore, it should be noted that the passive surface's interfacial capacitance (C_{WE2} and C_{WE1}) is presented as an ideal capacitor, while in fact it is often a function of the potential, the electrolyte's concentration and the frequency of the excitation voltage. In particular, the neglected frequency dependency of the electrical components in the model could be among the reasons for the poorer agreement in the case of the faster transients in the high-σ experiments [55].

The current study demonstrated that the charge needed for repassivation was temporarily obtained from the rapid discharge of the passive surface interfacial capacitance rather than from the concurrent cathodic current of the slow oxygen reduction. It is known that in the passivation process the cathodic current density has to exceed the critical current density i_{crit} [56,57]. As the capac-

itance is proportional to the area, we would expect that a scratch on a large electrode is more likely to repassivate, perhaps even under conditions where spontaneous repassivation is not expected.

When the described approach concerning the scratched-electrode technique under open-circuit conditions is compared to the common potentiostatic one, it is clear that the earlier one better resembles the field conditions. It can be argued that for neutral electrolytes with slow cathodic processes a potentiostat can provide an unrealistic supply of cathodic charge that results in a very short repassivation time of the order of a few ms. It should be noted that rapid repassivation conditions are ensured under open-circuit conditions when a large electrode is scratched and the change of the electrode potential is minor. Evidently, in both cases a certain fraction of the repassivation charge is obtained from the reservoir: a potentiostat or the passive surface's interfacial capacitance. A rather different situation occurs in the guillotined-electrode experiment, where the entire repassivation charge is provided only by the concurrent cathodic reactions [20]. The rate of current decay is indeed very slow (≈ 1 s for decay to 1/100 of the initial value), despite the highly conductive electrolyte. However, also under the open-circuit conditions of the scratching experiment when the area of the scratch is non-negligible compared to the entire surface area of the electrode, the conditions could differ substantially compared to the potentiostatic ones. Even in our experimental conditions, where the ratio between the scratch surface and the electrode surface was very small (0.0011 for the single-WE and 0.0003 for the dual-WE configuration), relatively high potential transients were obtained. It can, therefore, be argued that the scratched-electrode technique under potentiostatic conditions does not necessarily reflect the real field conditions.

6. Conclusions

In the present study a three-electrode experimental setup similar to the one for electrochemical noise measurements was used to measure the transients of the current and the coupled potential after a rapid single scratch on the passive surface in a neutral electrolyte. In contrast to most other studies, these measurements were made under open-circuit conditions that normally occur in the field. The measured transients were analyzed and modelled, to characterize the main electrochemical parameters that contribute to these transients.

Differences between the transients obtained in the low-σ and high-σ neutral electrolytes were observed. A comprehensive model based on the equivalent electrical circuit was developed where each circuit element has a clear relationship with a particular electrochemical property of the measured processes. To quantify the basic circuit elements, the transients measured in the single-WE system were analyzed. These values were thereafter implemented in the more general model for the dual-WE system. The model reproduces all the qualitative features of the experimental $E(t)$ and $I(t)$ curves and is also fairly accurate in quantitative predictions.

The interfacial capacitance of the electrodes was shown to have a crucial role in the characteristics of the observed potential and current transients. The major source of charge for the repassivation was proven to be the charge temporarily obtained from the passive surface's interfacial capacitance, rather than from the concurrent cathodic reactions. Due to the surface capacitance's dependence on the area, it would be expected that the scratch on the large electrode would, under certain circumstances, more likely repassivate compared to the one on the small-area electrode.

The developed model describes well the current and potential signal measurements after a rapid single scratch on the passive surface in a neutral electrolyte under open-circuit conditions. It is particularly accurate for a low-σ electrolyte, where the solution resistance is the major obstacle to the charge transfer. The

weaker agreement for the transients obtained in a high-σ electrolyte was primarily ascribed to the absence of a variable resistance due to oxide-layer growth in the model. When the model is complemented with a linear time-dependent resistance element, the agreement is significantly improved. The established model provided a clear interpretation of the electrochemical transients obtained under open-circuit conditions and tried to indicate the differences with respect to potentiostatically controlled systems.

Declaration of Competing Interest

The authors declare that they have no known competing financial interests or personal relationships that could have appeared to influence the work reported in this paper.

Credit authorship contribution statement

Bojan Zajec: Investigation, Validation, Visualization, Writing – original draft. **Tadeja Kosec:** Conceptualization, Visualization, Supervision, Funding acquisition, Writing – review & editing. **Andraž Legat:** Conceptualization, Funding acquisition, Writing – review & editing.

Acknowledgments

References

[1] D.D. Macdonald, Mechanism of depassivation, ECS Trans. 50 (31) (2013) 469–482.

[2] R. Carranza, J. Galvele, Repassivation kinetics in stress corrosion cracking – I. Type AISI 304 stainless steel in chloride solutions, Corros. Sci. 28 (3) (1988) 233–249.

[3] J. Scully, The interaction of strain-rate and repassivation rate in stress corrosion crack propagation, Corros. Sci. 20 (8–9) (1980) 997–1016.

[4] H. Kwon, E. Cho, K. Yeom, Prediction of stress corrosion cracking susceptibility of stainless steels based on repassivation kinetics, Corrosion 56 (1) (2000) 32–40.

[5] N. Papageorgiou, S. Mischler, Electrochemical simulation of the current and potential response in sliding tribocorrosion, Tribol. Lett. 48 (3) (2012) 271–283.

[6] M. Hashimoto, S. Miyajima, T. Murata, A stochastic analysis of potential fluctuation during passive film breakdown and repair on iron, Corros. Sci. 33 (6) (1992) 885–904.

[7] G. Frankel, B. Rush, C. Jahnes, C. Farrell, A. Davenport, H. Isaacs, Repassivation transients measured with thin film breaking electrodes, J. Electrochem. Soc. 138 (2) (1991) 643–644.

[8] S. Frangini, C. Piconi, Repassivation rates of surgical implant alloys by rotating-disk scratching measurements, Mater. Corros. Werkst. Korros. 52 (5) (2001) 372–380.

[9] G. Burstein, P. Marshall, Growth of passivating films on scratched 304L stainless steel in alkaline solution, Corros. Sci. 23 (2) (1983) 125–137.

[10] G. Burstein, G. Gao, Verification of the validity of peak bare surface current densities obtained from the scratched electrode, J. Electrochem. Soc. 138 (9) (1991) 2627–2630.

[11] P. Bastek, R. Newman, R. Kelly, Measurement of passive film effects on scratched electrode behavior, J. Electrochem. Soc. 140 (7) (1993) 1884–1889.

[12] D. Kolman, J. Scully, Limitations of potentiostatic repassivation techniques and their relationship to the applicability of the high field approximation to the repassivation of titanium, J. Electrochem. Soc. 142 (7) (1995) 2179–2188.

[13] G. Burstein, D. Davies, The electrochemical behavior of scratched iron surfaces in aqueous solutions, J. Electrochem. Soc. 128 (1) (1981) 33–39.

[14] R. Oltra, P. Bucaille, M. Indrianjafy, Modelling the capacitive behaviour of the passive film, in: K.R. Threthewey, P. Roberge (Eds.), Modelling Aqueous Corrosion: From Individual Pits to System Management, volume 266, Springer Science & Business Media, 1994, pp. 279–295.

[15] P. Jemmely, S. Mischler, D. Landolt, Electrochemical modeling of passivation phenomena in tribocorrosion, Wear 237 (1) (2000) 63–76.

[16] G. Burstein, K. Sasaki, Electrochemical reactions of freshly bared metal surfaces using the fluid impacted guillotined electrode, J. Electrochem. Soc. 148 (7) (2001) B282–B287.

[17] S. Mischler, Triboelectrochemical techniques and interpretation methods in tribocorrosion: a comparative evaluation, Tribol. Int. 41 (7) (2008) 573–583.

[18] D. Landolt, S. Mischler, M. Stemp, Electrochemical methods in tribocorrosion: a critical appraisal, Electrochim. Acta 46 (24) (2001) 3913–3929.

[19] R. Bosch, B. Schepers, M. Vankeerberghen, Development of a scratch test in an autoclave for the measurement of repassivation kinetics of stainless steel in high temperature high pressure water, Electrochim. Acta 49 (17) (2004) 3029–3038.

[20] G. Burstein, R. Cinderey, The potential of freshly generated metal surfaces determined from the guillotined electrodea new technique, Corros. Sci. 32 (11) (1991) 1195–1211.

[21] R. Oltra, G. Indrianjafy, M. Keddam, Current and potential transients during mechanical depassivation of passive iron, in: Materials Science Forum, volume 44, Trans Tech Publ, 1989, pp. 259–270.

[22] S. Mischler, S. Debaud, D. Landolt, Wear-accelerated corrosion of passive metals in tribocorrosion systems, J. Electrochem. Soc. 145 (3) (1998) 750–758.

[23] W. Oelssner, F. Berthold, U. Guth, The IR drop–well-known but often underestimated in electrochemical polarization measurements and corrosion testing, Mater. Corros. 57 (6) (2006) 455–466.

[24] A.J. Davenport, B.K. Lee, Passive film growth kinetics for iron and stainless steel, in: Proceedings of the Electrochemical Society, volume 13, 2002, pp. 187–197.

[25] G. Burstein, R. Cinderey, Evolution of the corrosion potential of repassivating aluminium surfaces, Corros. Sci. 33 (3) (1992) 475–492.

[26] R. Cinderey, G. Burstein, The repassivation potential of aluminium in water, Corros. Sci. 33 (3) (1992) 499–502.

[27] Z. Chen, The open-circuit potential of a polarizable and reactive electrode, ECS Trans. 6 (24) (2008) 1–15.

[28] M. Stoudt, A. Vasudevan, R. Ricker, Examination of the influence of lithium on the repassivation rate of aluminum alloys, in: New Methods for Corrosion Testing of Aluminium Alloys Philadelphia (PA/USA)(Proc. Conf.), ASTM STP, volume 1134, 1992, pp. 196–213.

[29] R. Cottis, Interpretation of electrochemical noise data, Corrosion 57 (3) (2001) 265–285.

[30] A. Legat, V. Doleček, Chaotic analysis of electrochemical noise measured on stainless steel, J. Electrochem. Soc. 142 (6) (1995) 1851.

[31] A. Legat, J. Osredkar, V. Kuhar, M. Leban, Detection of various types of corrosion processes by the chaotic analysis of electrochemical noise, in: Materials Science Forum, volume 289, 1998, pp. 807–812.

[32] M. Leban, V. Doleček, A. Legat, Electrochemical noise during non-stationary corrosion processes, Mater. Corros. 52 (6) (2001) 418–425.

[33] A. Legat, V. Dolecek, Corrosion monitoring system based on measurement and analysis of electrochemical noise, Corrosion 51 (4) (1995) 295–300.

[34] H.S. Isaacs, C. Scheffey, R. Huang, The location of events producing potential transients during pitting of freely corroding Al and its alloys, ECS Trans. 11 (22) (2008) 1–12.

[35] K. Sasaki, H. Isaacs, Origins of electrochemical noise during pitting corrosion of aluminum, J. Electrochem. Soc. 151 (3) (2004) B124–B133.

[36] G. Berthomé, B. Malki, B. Baroux, Pitting transients analysis of stainless steels at the open circuit potential, Corros. Sci. 48 (9) (2006) 2432–2441.

[37] H.S. Klapper, B. Zajec, A. Heyn, A. Legat, Elucidating nucleation stages of transgranular stress corrosion cracking in austenitic stainless steel by in situ electrochemical and optical methods, J. Electrochem. Soc. 166 (11) (2019) C3326–C3335.

[38] J. Kovac, C. Alaux, T.J. Marrow, E. Govekar, A. Legat, Correlations of electrochemical noise, acoustic emission and complementary monitoring techniques during intergranular stress-corrosion cracking of austenitic stainless steel, Corros. Sci. 52 (6) (2010) 2015–2025.

[39] J. Kovač, M. Leban, A. Legat, Detection of SCC on prestressing steel wire by the simultaneous use of electrochemical noise and acoustic emission measurements, Electrochim. Acta 52 (27) (2007) 7607–7616.

[40] M. Leban, V. Doleček, A. Legat, Comparative analysis of electrochemical noise generated during stress corrosion cracking of AISI 304 stainless steel, Corrosion 56 (9) (2000) 921–927.

[41] Y. Ge, X. Xie, J. Roscher, R. Holze, Q. Qu, How to measure and report the capacity of electrochemical double layers, supercapacitors, and their electrode materials, J. Solid State Electrochem. 24 (11) (2020) 3215–3230.

[42] L.E. Helseth, Comparison of methods for finding the capacitance of a supercapacitor, J. Energy Storage 35 (2021) 102304.

[43] H.S. Isaacs, J.-H. Cho, Potential transmission and transients during corrosion: applications to corrosion monitoring, Corros. Sci. 35 (1–4) (1993) 97–101.

[44] H. Isaacs, "A stochastic analysis of potential fluctuations during passive film breakdown and repair of iron": by M. Hashimoto, S. Miyajima and T. Murata (pp 885904, vol. 33, no. 6, 1992), Corros. Sci. 34 (3) (1993) 525–528.

[45] R. Oltra, G. Indrianjafy, R. Roberge, Effect of electrical transient coupling phenomena on the initiation of pits by a pulsed laser, J. Electrochem. Soc. 140 (2) (1993) 343.

[46] E. Cho, C.-K. Kim, J.-S. Kim, H.-S. Kwon, Quantitative analysis of repassivation kinetics of ferritic stainless steels based on the high field ion conduction model, Electrochim. Acta 45 (12) (2000) 1933–1942.

[47] T. Adler, R. Walters, Corrosion and wear of 304 stainless steel using a scratch test, Corros. Sci. 33 (12) (1992) 1855–1876.

[48] H. Pearson, G. Burstein, R. Newman, Resistance to flow of current to scratched electrodes, J. Electrochem. Soc. 128 (11) (1981) 2297–2303.

[49] Ngspice online, Accessed: 29-09-2021, http://ngspice.sourceforge.net/.

[50] M. Danielson, Modeling of certain electrode parameters on the electrochemical noise response, Corrosion 53 (10) (1997) 770–777.

[51] J. Jeans, The Mathematical Theory of Electricity and Magnetism, Cambridge University Press, 1960.

[52] P. Doig, P. Flewitt, An analysis of galvanic corrosion: coplanar electrodes with one electrode infinitely large, Philos. Mag. B 38 (1) (1978) 27–40.

[53] W. Schwerdtfeger, I.A. Denison, Geometric factors in electrical measurements relating to corrosion and its prevention, Corrosion 11 (10) (1955) 25–34.

[54] H.S. Isaacs, A.J. Davenport, The influence of surface capacitance on the measurements of localized corrosion transients, J. Electrochem. Soc. 137 (7) (1990) 2196–2198.

[55] J. Newman, Frequency dispersion in capacity measurements at a disk electrode, J. Electrochem. Soc. 117 (2) (1970) 198–203.

[56] R.G. Kelly, J.R. Scully, D. Shoesmith, R.G. Buchheit, Electrochemical Techniques in Corrosion Science and Engineering, CRC Press, 2002.

[57] H.S. Klapper, J. Göllner, A. Heyn, A. Burkert, Relevance of the cathodic process on the passivation of stainless steels–an approximation to the origin of the rouging phenomenon, Mater. Corros. 63 (1) (2012) 54–58.